Inorganic Chemistry

Article

pubs.acs.org/IC

Tetranuclear Silver(I) Clusters Showing High Ionic Conductivity in a Bicontinuous Cubic Mesophase

Padi Y. S. Su,[†] Jing C. W. Tseng,[†] Kwang-Ming Lee,[‡] Ju-Chun Wang,[§] and Ivan J. B. Lin*[,†]

[†]Department of Chemistry, National Dong Hwa University, No. 1, Section 2, Da Hsueh Road, Shoufeng, Hualien 97401, Taiwan

[‡]Department of Chemistry, National Kaohsiung Normal University, 62 Shen-Shung Road, Kaohsiung 82444, Taiwan

[§]Department of Chemistry, Soochow University, No. 70, Lin Shih Road, Shih-Lin, Taipei 11102, Taiwan

Supporting Information

ABSTRACT: The synthesis and characterization of tetranuclear silver triazole metallomesogens, $[Ag_4(L^4\text{-}C_n)_6][BF_4]_4$ ($L^4\text{-}C_n$ = 4-alkyl-1,2,4-triazoles where C_n stands for C_nH_{2n+1} with n = 12, 14, 16, and 18), are reported. Upon heating, a phase transition sequence of Cr → SmC → Cub → SmA → isotropic liquid is observed for all of these compounds. Depending on the alkyl chain length, two types of cubic phases are found in this series of compounds. Those with shorter alkyl chains (n = 12 and 14) exhibit a micellar cubic phase, whereas long alkyl chains (n =16 and 18) show a bicontinuous cubic phase. Superior ionic conductivity at the bicontinuous cubic mesophase for $[Ag_4(L_4\text{-}C_{16})_6][BF_4]_4$ is observed because of the presence of a three-dimensional ion-transporting channel. Doping a small amount of $AgBF_4$ enhances the ionic conduction dramatically, presumably via promotion of the migration of Ag^I ions in the channels.

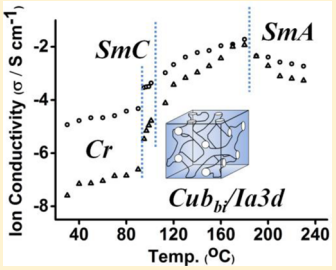

1. INTRODUCTION

Although the development of thermotropic liquid crystals (LCs) has a long history, thermotropic cubic phases have been less understood in terms of the relationship between the molecular morphology and mesophase structure.[1−5] It is not an easy task to predict the structure of the cubic phase simply from the shape of the molecules. Recent advancement suggests that the shape of the interfaces resulting from intermolecular interactions is the key to understanding of the mesophase structure. Two types of cubic phases have been commonly observed: a micellar cubic phase (Cub_{dis}) and a bicontinuous cubic phase (Cub_{bi}).[4,6−10] In the former, discontinuous micelles are arranged in a cubic lattice. In the latter, the cubic lattice has a three-dimensional (3D) interwoven network.[11−16] The features of a 3D nanochannel network may provide many interesting properties. For example, with ionic constituents, these 3D channels could facilitate the transportation of ions without the need of alignment, compared to the smectic[7,12−14] and columnar phases.[15,17−19] They thus could show high ionic conductivities. Neutral constituents with ligating functional groups in the channel could also be used as ion-transporting materials via doping of ionic compounds.

Metallomesogens are LCs containing metal ions as part of their compositions.[3,20−31] Metallomesogens provide the LCs with additional properties possessed by the metal ions, such as magnetism, geometry, color, emission, redox behavior, and so on.[21,32−44] Metallomesogens are also known to form thermotropic cubic phases.[25,45−50] The most intensively studied systems are the silver(I) alkoxystilbazole complexes.[25] Through tuning of the chain number, chain length, and anion, these compounds show rich and diverse mesomorphism and have been nicely reviewed.[25] Other examples, such as ferrocene-containing hexacatenar metallomesogens,[46] organometallic compounds of Cu^I, Au^I, Pd^{II}, and Pt^{II} via coordination with a second generation dendritic isocyanide,[45] and sandwich-type phthalocyanine-based rare-earth metal complexes of europium, terbium, and lutetium are also known to form cubic phases.[51]

4-Alkyl-1,2,4-triazoles have been used as bridging ligands to form metal complexes with rich morphologies and properties.[37,39,41−44,52−55] For example, one-dimensional (1D) iron(II) triazole complexes have been reported to show interesting spin-crossover phenomena, photoinduced morphological transformation, and/or liquid-crystalline behaviors.[41,52−54,56] Coordination polymers of zinc(II) triazole with liquid-crystalline properties[52] and cobalt(II) triazole showing gellating and coordination structure transformation behaviors have also been known.[38,41] Coordination of triazoles to the Ag^I ion could form complexes with diverse structures because of the rich variation in the coordination numbers.[57−66] For example, four-coordinated Ag^I ions could form 1D coordination polymers with triazole ligands, and three-coordinated Ag^I ions form discret tetranuclear complexes.[63−66]

We have been interested in LCs of silver(I) complexes. Most of the systems that we have studied exhibit SmA mesophases. It is our intention to look for silver(I) complexes showing different mesophases. In this work, LCs of silver(I) triazole complexes with the stoichiometry of $[Ag_4(triazole)_6][BF_4]_4$ are reported. These compounds, comprising a planar tetranuclear silver(I) cluster and six bridging 4-alkyl-1,2,4-triazole ligands, display thermotropic LCs with the phase transition sequence of Cr → SmC → Cub → SmA → isotropic liquid. Cubic

Received: November 14, 2013
Published: June 3, 2014

   dx.doi.org/10.1021/ic500627d | Inorg. Chem. 2014, 53, 5902−5910

Scheme 1. Synthetic Pathways and Abbreviations for the Ligands and Compounds

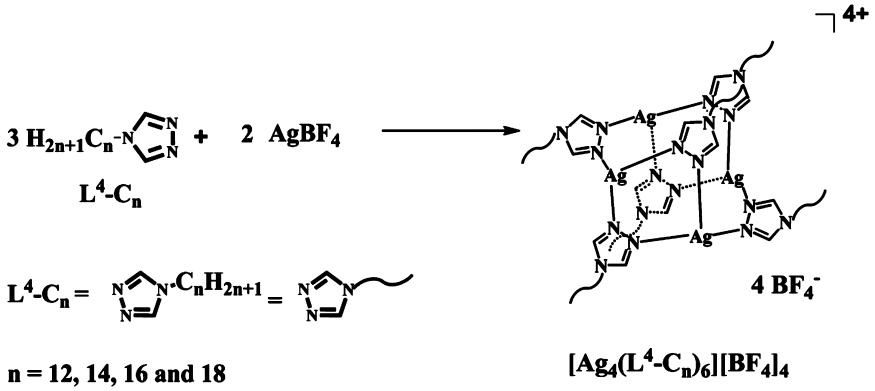

mesophases of either Cub_{bi} or Cub_{dis} are observed depending on the alkyl chain lengths of the compounds. Compounds in the thermotropic Cub_{bi} phase, especially when doped with a small amount of $AgBF_4$, demonstrate superior ionic conductivities compared to most of the other compounds in the Cub_{bi} phase.

2. RESULTS AND DISCUSSION

Compounds of $[Ag_4(L^4\text{-}C_n)_6][BF_4]_4$ ($L^4\text{-}C_n$ = 4-alkyl-1,2,4-triazoles, where C_n stands for C_nH_{2n+1} with n = 12, 14, 16, and 18) are prepared by stirring a mixture of 3 equiv of $L^4\text{-}C_n$ in CH_2Cl_2 with 2 equiv of $AgBF_4$ in methanol (MeOH) at room temperature. Interestingly, the known tetranuclear triazole (Ag_4-triazole) complexes were isolated accidentally when 1:1 and 2:1 molar ratios of ligand to silver(I) were employed.[63−66] The reaction and formation of these complexes are schematically shown in Scheme 1.

Crystals of $[Ag_4(L^4\text{-}C_{14})_6][BF_4]_4$ are obtained by the diffusion of diethyl ether into a dichloromethane solution at room temperature. The ORTEP diagram of this compound is given in Figure 1a. The four Ag^I ions in the central core form a parallelogram, similar to those reported.[65,66] The lengths of the two sides in the parallelogram are 3.450 and 3.792 Å. These values are compared to those complexes with ClO_4^- (3.396 and 3.732 Å) and NO_3^- (3.714 and 3.905 Å) anions.[65,66] The Ag−N bond lengths of this compound are in the range between 2.10 and 2.50 Å and are normal. In the central framework, a pair of Ag^I ions are bridged by two L^4 ligands to form a six-membered metalloring of $[N_2Ag_2N_2]$ with a long Ag1···Ag2 distance of 3.792 Å. Further, two of these units are cyclized via two bridging L^4 ligands with a shorter Ag1···Ag2A distance of 3.450 Å. Each Ag^I cation is three-coordinated with three N-donor atoms. Viewed along the Ag1−Ag2 axis, the dihedral angles between the two triazole planes are 164.0°, compared to the literature value of 171.5° or 173.3°.[63,66] One can consider that the ionic rigid core is composed of six triazole rings encapsulating four silver ions (Figure 1b). Connecting the six N^4 atoms shows an antiprismatic morphology, in which the triangular face has lengths of 6.998, 5.736, and 4.301 Å, and the two planes are separated by ∼6.92 Å (Figure 1c,d). This rodlike cationic core makes an angle of ∼45° with respect to the chains. The lamellar structure is thus formed via a monolayer assembly of the cations with interdigitated alkyl chains (Figure 1e). This structure gives a layer spacing of 25.6 Å compared to the molecular length of 42.2 Å. Details of the crystal data are given in Table 1. Selected bond lengths and angles are provided in Table S1 in the Supporting Information (SI). All of this information has been deposited at the Cambridge Crystallographic Data Center as CCDC 942251.

These tetranuclear silver triazole complexes exihibit rich mesomorphism. Details of the phase transition temperatures with accompanying thermodynamic data are given in Table 2 and Figure 2. The thermotropic phase behavior for the compound of n = 12 will be discussed first. The profile of differential scanning calorimetry (DSC) for this compound (Figure 3) shows that, upon heating from the crystal phase (Cr), the first phase transition occurs at 70.6 °C with an enthalpy change of 78.4 kJ/mol. This phase persists up to 121.0 °C, at which a second phase transition appears with a smaller enthalpy change of 11.8 kJ/mol. The third phase transition happens at 190.6 °C with an enthalpy value of 19.2 kJ/mol. Finally, a transition to isotropic liquid appears at 212.9 °C, with a corresponding endothermic enthalpy value of 4.1 kJ/mol. Partial decomposition occurs upon isotropization, such that the phase transition temperatures in the cooling process are not reproducible. Therefore, only the heating thermogram is provided. Polarized optical microscopy (POM) is employed to assign these mesophases. At 95 °C in the first mesophase, schlieren texture without a homeotropic region is found (Figure 3a), and thus a SmC phase is tentatively assigned. The next mesophase between 121.0 and 190.6 °C is completely dark under POM (Figure 3b), suggesting that this phase is optically isotropic. We attempt to assign this phase as the cubic phase (Cub), which will be further characterized from the study of powder X-ray diffraction (PXRD). Between 190.6 and 212.9 °C, in the third mesophase, a focal conic texture together with homeotropic domains is observed, which is typical for a SmA mesophase found in ionic LCs (Figure 3c). Similarly, for the homologous compounds of n = 14, 16, and 18, the phase transitions from Cr to SmC, Cub, and then SmA are observed.

Small-angle X-ray scattering (SAXS) analysis is performed to understand the molecular arrangement of these compounds at different phases. For the compound of n = 12, a layer distance of 23.1 Å is observed at the solid state. Upon transition to SmC, the layer distance increases to 25.5 Å at 80 °C. In the same mesophase, the layer distance further increases to 25.7 Å at 90 °C and 25.8 Å at 100 °C (Figure S1 in the SI). This temperature-dependent behavior is consistent with the assignment of SmC, where the director tilting angle with respect to the layer normal decreases upon increasing temperature.[67] In the Cub phase at 160 °C, there are two intense peaks followed by six weak peaks, which correspond to distances of 30.8, 27.7, 15.4, 13.9, 12.0, 11.2, 10.3, and 9.5 Å (Figure 4). These spacings are in the reciprocal ratio of $\sqrt{4}$, $\sqrt{5}$, $\sqrt{16}$, $\sqrt{20}$,

dx.doi.org/10.1021/ic500627d | Inorg. Chem. 2014, 53, 5902−5910

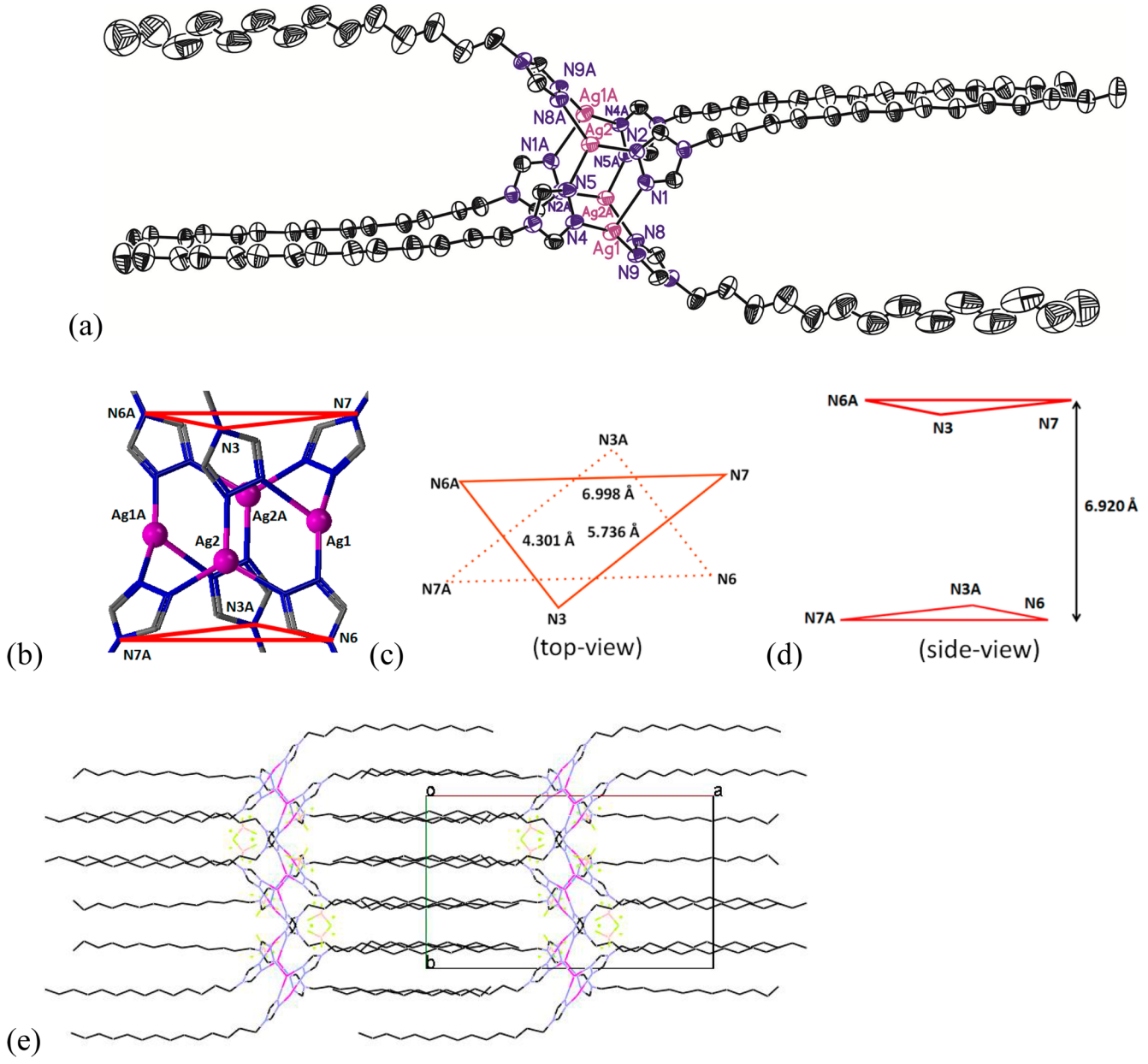

Figure 1. (a) ORTEP drawing with atomic labeling for the cation of $[Ag_4(L^4\text{-}C_{14})_6][BF_4]_4$ (30% thermal ellipsoids). H atoms and BF_4^- anions are omitted for clarity. (b) Ionic rigid core composed of six triazole rings encapsulating four silver ions (Ag1 and Ag2, *x*, *y*, *z*; Ag1A and Ag2A, 1 − *x*, 1 − *y*, 1 − *z*), connecting the six N^4 atoms showing an antiprismatic morphology. (c) Top view of the antiprism, in which the triangular face has lengths of N3···N7 (N3A···N7A) = 5.735 Å, N6A···N7 (N6···N7A) = 6.998 Å, and N3···N6A (N3A···N6) = 4.301 Å. N3, N6, and N7: *x*, *y*, *z*. N3A, N6A, and N7A: 1 − *x*, 1 − *y*, 1 − *z*. (d) Side view of the antiprism showing a separation of ∼6.92 Å between the two planes. (e) Monolayer stacking with interigitated alkyl chains viewed along the *c* axis.

$\sqrt{26}$, $\sqrt{30}$, $\sqrt{36}$, and $\sqrt{42}$ and are indexed in sequence as (200), (210), (400), (420), (510), (521), (442), and (541) reflections. This leads to an assignment of $Cub_{dis}/Pm3n$ symmetry with a lattice parameter of a = 61.6 Å.[68,69] Although a $Pm3n$ lattice often shows three dominating (200), (210), and (211) reflections, examples with one or two of these reflections missing are known.[69−73] The relative intensity of the (200) and (210) reflections is temperature-dependent. Upon heating, the intensity of the (200) reflection decreases, whereas that of the (210) reflection increases. Finally, in the SmA mesophase, a d_{100} spacing of 27.7 Å is observed at 194 °C, and it then decreases gradually to 27.6 Å at 196 °C and 27.4 Å at 198 °C. The observation of a gradual decrease in the d spacing upon increasing temperature is presumably due to an increasing thermal motion of the alkyl chains and is consistent with a SmA phase. Temperature-dependent SAXS diffractograms for the compound of n = 12 are given in Figure S1 in the SI. The homologous compound of n = 14 has similar SAXS results, and theses are provided in Table S2 and Figure S2 in the SI.

For the compound of n = 16, a layer distance of 28.1 Å is observed at the solid state. The layer spacing in the SmC phase can not be obtained because its narrow mesophase range lies between two overlapping endothermic processes. The SAXS reflection pattern of this compound in the cubic phase is different from that for the compounds of n = 12 and 14. At 160 °C, there are two intense peaks followed by seven weak peaks,

dx.doi.org/10.1021/ic500627d | *Inorg. Chem.* 2014, 53, 5902−5910

Table 1. Crystal Data and Structure Refinements for $[Ag_4(L^4\text{-}C_{14})_6][BF_4]_4$

complex	$[Ag_4(L^4\text{-}C_{14})_6][BF_4]_4$
empirical formula	$C_{96}\ H_{186}\ Ag_4\ B_4\ F_{16}\ N_{18}$
fw	2371.35
temperature (K)	273(2)
wavelength (Å)	0.71073
cryst syst	monoclinic
space group	$P2(1)/c$
a (Å)	25.605(4)
b (Å)	15.317(3)
c (Å)	15.290(3)
α (deg)	90
β (deg)	93.782(5)
γ (deg)	90
V (Å^3)	5983.5(17)
Z	2
calcd density (mg/m^3)	1.316
abs coeff (mm^{-1})	0.717
F(000)	2480
θ range for data collection (deg)	1.55−29.04
reflections collected/unique	96348/15798 [R(int) = 0.0529]
completeness to θ (%)	99.00
data/restraints/param	15798/253/670
GOF on F^2	1.064
final R indices [$I > 2(I)$]	R1 = 0.0431, wR2 = 0.1065
R indices (all data)	R1 = 0.1063, wR2 = 0.1308
largest diff peak and hole (e/Å^3)	0.518 and −0.376

Table 2. Phase Transition Behavior of $[Ag_4(L^4\text{-}C_n)_6][BF_4]_4$

compound	n	phase transition behavior and T [ΔH][a]
$[Ag_4(L^4\text{-}C_n)_6][BF_4]_4$	12	Cr 70.6[78.4] SmC 121.0[11.8] Cub_{dis}/$Pm3n$ 190.6[19.2] SmA 212.9[4.1] I_d
	14	Cr 84.7[129.9] SmC 119.1[12.4] Cub_{dis}/$Pm3n$ 187.9[27.6] SmA 230.2[4.7] I_d
	16	Cr 94.4[150.1] SmC 110.1[5.4] Cub_{bi}/$Ia3d$ 179.8[18.6] SmA 226.3[4.9] I_d
	18	Cr 100.2[156.9] SmC 118.9[5.0] Cub_{bi}/$Ia3d$ 177.1[18.8] SmA 224.0[5.0] I_d

[a]Cr = crystal phase; SmA = smectic A phase; SmC = smectic C phase; Cub_{dis} = micellar cubic phase; Cub_{bi} = bicontinuous cubic phase; I = isotropic; d = decomposition, deteced by POM. The phase transition temperatures (°C) and enthalpies (in parentheses, kJ/mol) are determined by the DSC thermogram at a scan rate of 10.0 °C/min.

corresponding to d spacings of 38.1, 33.2, 19.0, 16.6, 12.7, 11.9, and 11.1 Å, as shown in Figure 5. These observed d spacings are in the reciprocal ratio of $\sqrt{6}$, $\sqrt{8}$, $\sqrt{24}$,$\sqrt{32}$, $\sqrt{54}$, $\sqrt{62}$, and $\sqrt{72}$ and are indexed in sequence as (211), (220), (422), (440), (721), (651), and (660) reflections, which fit the Cub_{bi} mesophase with $Ia3d$ symmetry of a = 93.3 Å. The relative intensity of (211) and (220) is also temperature-dependent; upon increasing temperature, the intensity of the (220) reflection increases, whereas the (211) reflection decreases in intensity. This temperature-dependent behavior is also observed in the silver stilbazole system.[74] In the SmA mesophase, a d_{100} spacing of 32.6 Å is observed at 194 °C. The compound of n = 18 has a similar temperature-dependent behavior, and it is provided in Table S2 and Figure S3 in the SI.

In the Cr phase, compounds of n = 12, 14, 16, and 18 show a steady increase (Figure 6) of the layer spacing from 23.1 to 25.6, 28.1, and then 30.8 Å. This observation suggests that these compounds have crystal structures similar to that found for the compound of n =14, a monolayer molecular assembly with interdigitated alkyl chains. From the Cr to SmC phase, there is a slight increase in the layer spacing, for example, from 23.1 to 25.7 Å for the compound of n =12. The slight increase in the d spacing is presumably due to a change of the molecular arrangement from interdigitated to partially interdigitated alkyl chains, while the molecular rods tilt with respect to the normal of the layer plane and pack in a monolayer assembly. The structure of SmA will be discussed before the cubic phase because the structure of SmA may give some clues to the structure of the cubic phase. In the SmA phases, the steady increase in the d spacing upon lengthing of the alkyl chain from n = 12 to 18 again suggests the similarity in structure. We will use the compound of n = 12 to illustrate the structure in SmA. A molecular length of 42.2 Å is measured from the crystal structure of the compound with n = 14. This leads to an estimation of the molecular length for the compound with n = 12 of 37.2 Å; this value is much longer that the layer distance of 27.6 Å of the SmA phase. Therefore, in this mesophase, the molecular rods are proposed to align perpendicularly to the layer plane, with the alkyl chains partially interdigitated.

Depending on the alkyl chain length, two types of cubic phases are found in this series of compounds. Those with shorter alkyl chains (n = 12 and 14) exhibit a $Pm3n$ micellar cubic phase, whereas those with long alkyl chains (n =16 and 18) show a $Ia3d$ bicontinuous cubic phase (Figure 7). Commonly, for a $Pm3n$ lattice, molecules are aggregated to form a micelle, eight of which are further organized to form a cubic arrangement. The number of molecules needed to form a sphere can be calculated from the total number of molecules in a unit cell (n_{cell}) divided by the number of aggregates. To estimate n_{cell}, eq 1 could be employed,[75,76] where V_{cell} is the volume of the unit cell from PXRD, N_A is Avogadro's constant, and M is molecular mass. As a common practice, one assumes a density (ρ) of 1 g/cm^3 in the calculation. The estimated n_{cell} values for the BF_4^- complexes of n = 12 and 14 are 64 and 80, respectively. Therefore, there are 8 and 10 molecules per micelle correspondingly. The number of molecules per micelle with only 8−10 is small compared to most of the known micellar cubic phases;[76−81] however, examples of micelles formed with small numbers of molecules are also known.[71,77] For the compound of n =12, the $Pm3n$ lattice dimension of 61.6 Å would give a micelle diameter of about 30.8 Å, assuming a rodlike micelle (half of the lattice dimension),[79,80] or ca. 38.0 Å, assuming a spherical micelle.[77] The former value is closer to the d values of ∼26.0 Å for the SmC or ∼28.0 Å for the SmA. In the rodlike micelle, a model of the molecular assembly with the ionic cores in the center and the alkyl chains pointing outward to form an inverted micelle is proposed (Figure 7). With longer chains, molecules of the compound with n = 16 are proposed to self-assemble with ions organized in the channels and alkyl chains in the continuum to form a $Ia3d$ bicontinuous cubic phase. This arrangement is supported by the ionic conduction behavior, which will be discussed in a later section.

$$n_{cell} = V_{cell}(N_A/M)\rho \quad (1)$$

The ionic conductivities of $[Ag_4(L^4\text{-}C_{14})_6][BF_4]_4$ and $[Ag_4(L^4\text{-}C_{16})_6][BF_4]_4$ are examined. The former has a Cub_{dis} phase, whereas the latter possesses a Cub_{bi} phase. The ionic conductivities are measured using two types of cells: comb-shaped gold electrodes and indium−tin oxide (ITO) electrodes.[82,83] With comb-shaped gold electrodes, the conductivities are measured along the glass surface. On the other hand, with

dx.doi.org/10.1021/ic500627d | Inorg. Chem. 2014, 53, 5902−5910

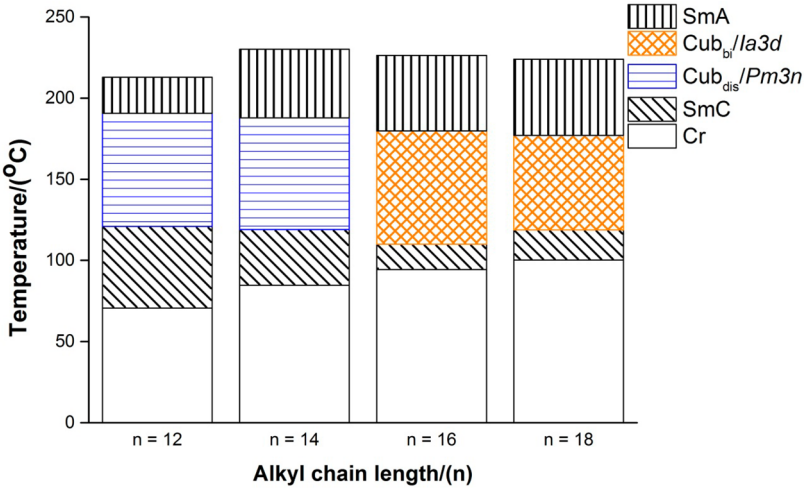

Figure 2. Comparison of the phase-transition temperature versus alkyl chain length for the $[Ag_4(L^4\text{-}C_n)_6][BF_4]_4$ series of compounds upon heating.

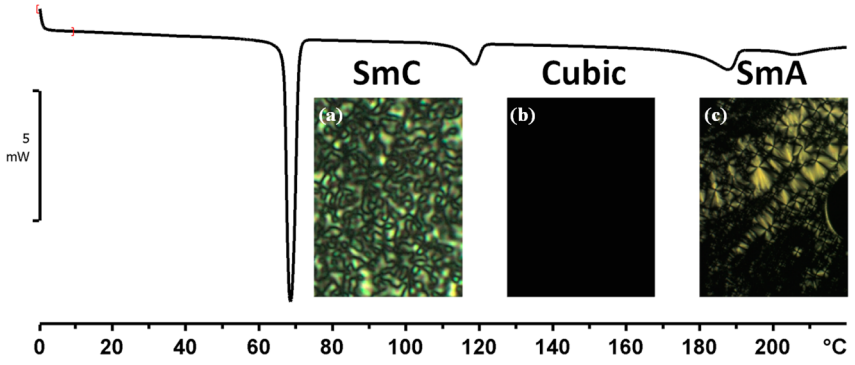

Figure 3. DSC thermogram of $[Ag_4(L^4\text{-}C_{12})_6][BF_4]_4$ with POM images taken at the (a) SmC mesophase (95 °C), (b) Cub mesophase (170 °C), and (c) SmA mesophase (195 °C) in the heating process.

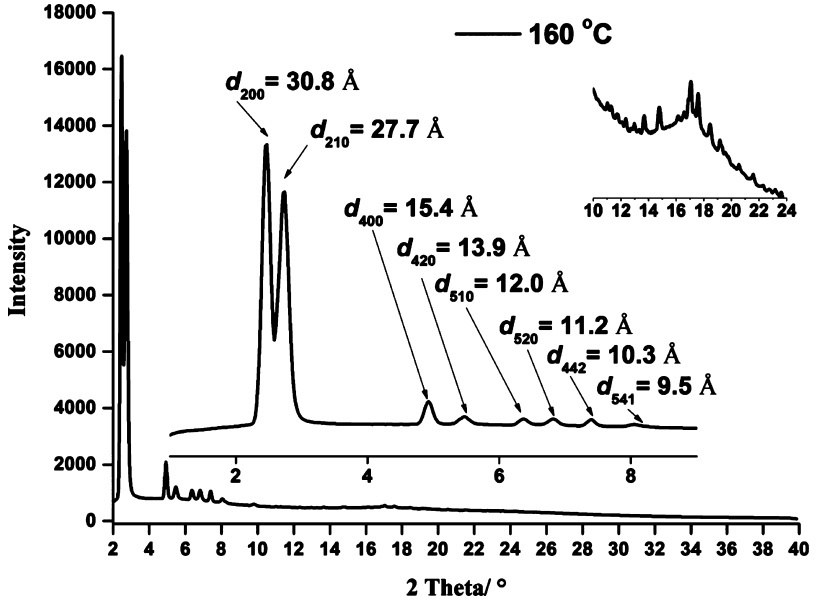

Figure 4. Diffractogram of the Cub$_{dis}$/*Pm*3*n* phase for $[Ag_4(L^4\text{-}C_{12})_6][BF_4]_4$ at 160 °C.

ITO electrodes, the conductivities are measured along the direction perpendicular to the glass surface.

The results of the ionic conductivities measured for the compounds of n = 14 and 16 at different temperatures are shown in Figure 8. Using comb-shaped gold electrodes, the ionic conductivity of $[Ag_4(L^4\text{-}C_{14})_6][BF_4]_4$ in the Cr phase increases slightly with increasing temperature. Upon transition to SmC at 95 °C, there is a sudden increase in the ionic conductivity, which further increases upon heating to 101 °C in the range of the SmC phase. From the SmC to Cub$_{dis}$ phase at

dx.doi.org/10.1021/ic500627d | *Inorg. Chem.* 2014, 53, 5902−5910

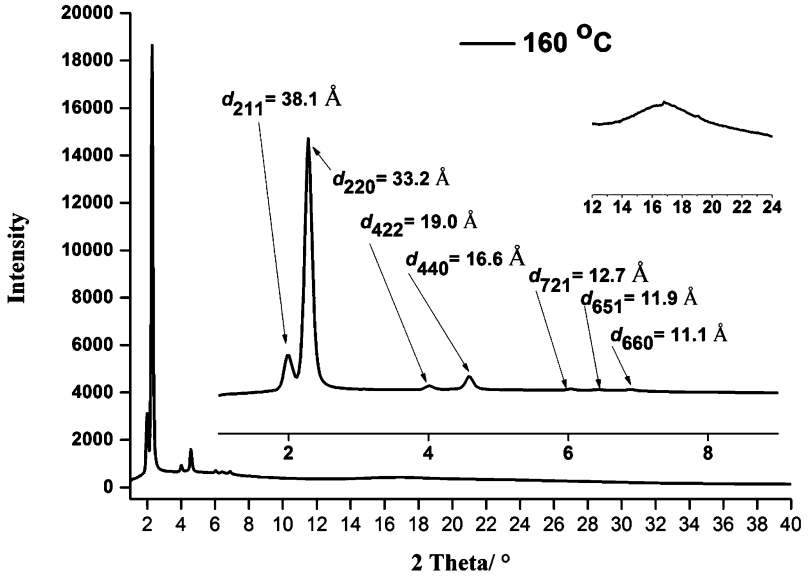

Figure 5. Diffractogram of the $Cub_{bi}/Ia3d$ phase for $[Ag_4(L^4\text{-}C_{16})_6][BF_4]_4$ at 160 °C.

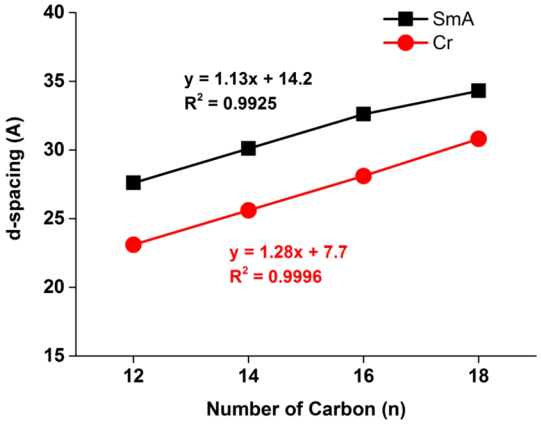

Figure 6. Plots of d spacing versus alkyl chain length for $[Ag_4(L^4\text{-}C_n)_6][BF_4]_4$ in the Cr and SmA phases.

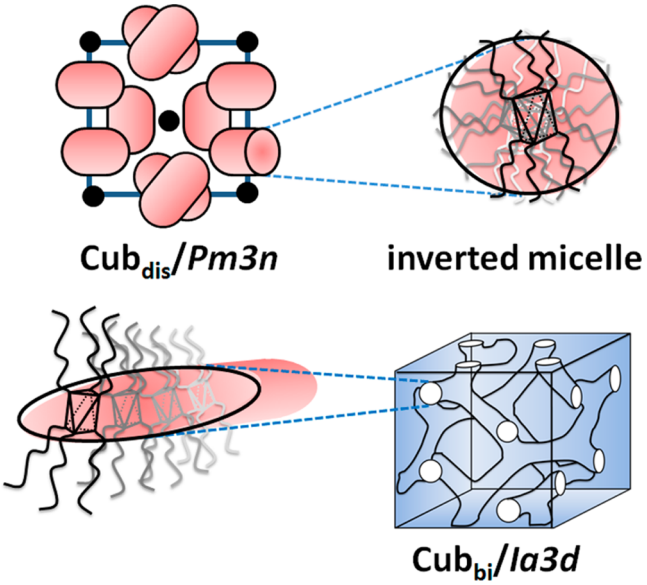

Figure 7. Schematic representation of the proposed self-assemblies in the micellar cubic phase ($Cub_{dis}/Pm3n$) and in the three interwoven networks of the bicontinuous cubic phase ($Cub_{bi}/Ia3d$).

120 °C, there is a sudden decrease in the ionic conductivity, which then increases gradually with increasing temperature. Upon transition to SmA, ionic conductivities first show a greater upsurge and then a smooth increase upon heating. These observations suggest that, other things being equal, the ion-conducting ability in the micellar cubic phase is inferior to that in the SmC and SmA phases, as have been reported.[16,80] If instead, a cell with ITO electrodes is utilized, two interesting points are observed. First, the measured ionic conductivities in all phases are found to be lower than those using comb-shaped gold electrodes, a nature due to the inherent conductivity of the electrodes. In addition, we notice that there is a smooth increase of the ionic conductivity from SmC to Cub_{dis} and then to SmA. The steady increase of the ionic conductivity with increasing temperature is understandable; the conductivity measured with ITO electrodes is in the direction perpendicular to the ionic and insulating layers in the SmC and SmA phases, a scenario similar to that for micelles in Cub_{dis}. This explains the continuum of ionic conductivities measured from SmC → Cub_{dis} → SmA with ITO electrodes but not with gold finger electrodes.

For the compound of $[Ag_4(L^4\text{-}C_{16})_6][BF_4]_4$, measurements using either gold finger or ITO electrodes give a similar trend of temperature-dependent ionic conduction. Higher values, however, are found using the former electrodes. The ionic conductivity values in the Cr and SmC phases are comparable to those of $[Ag_4(L^4\text{-}C_{14})_6][BF_4]_4$. On the other hand, a significant increase in the ionic conductivity is observed in the Cub_{bi} phase. Using gold finger electrodes, the highest ionic conductivity of 1.9×10^{-2} S/cm is observed at 178 °C. This value is almost 3 orders of magnitude greater than the conductivities found in the Cub_{dis} phase for n = 14. Upon transition from Cub_{bi} to SmA at 190 °C, there is a decrease in the ionic conductivity, supporting the expected superior ionic conduction in Cub_{bi}. Further, when a 0.5% molar ratio of $AgBF_4$ is doped to the compound of n = 16, an enhanced ionic conductivity (8.4×10^{-2} S/cm) of 4 times higher is observed in the Cub_{bi} phase (Figure S4 in the SI).

dx.doi.org/10.1021/ic500627d | Inorg. Chem. 2014, 53, 5902−5910

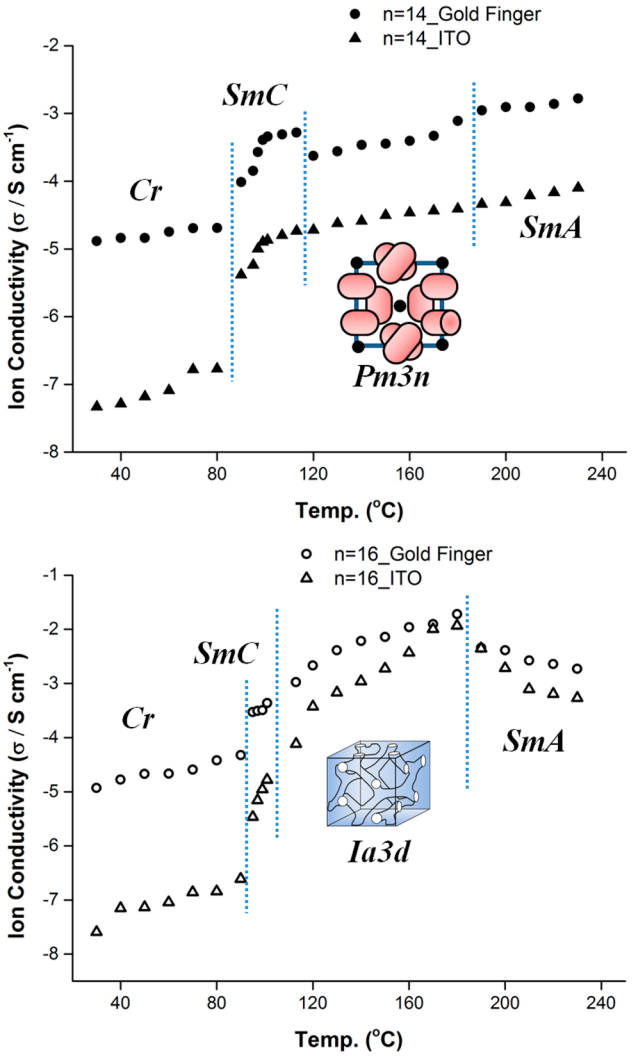

Figure 8. Ionic conductivities of $[Ag_4(L^4\text{-}C_n)_6][BF_4]_4$ (n = 14 and 16): for n = 14, (●) comb-shaped gold electrodes and (▲) ITO electrodes; for n = 16, (○) comb-shaped gold electrodes and (Δ) ITO electrodes.

The ion mobility in a confined nanostructure of the Cub_{bi} phase has been studied via pulsed-field-gradient NMR spectroscopy.[13] The compound studied consists of a fan-shaped ammonium cation and a tetrafluoroborate anion. In that experiment, while both ions migrate, anions diffuse twice as fast as the bulky cations. A similar mechanism probably applies to our system, in which ionic conduction is via transportation of the $[Ag_4(L^4\text{-}C_n)_6]^{4+}$ cation and the BF_4^- anion. The necessity to have mobile ions to show ionic conduction is illustrated by the reported LCs of silver stilbazole complexes; these compounds did not show ionic conduction in the $Cubb_{bi}$ phase. A reason due to coordination of the sulfate anion to the Ag^I ion has been proposed.[84] We also notice that the ionic conductivities found in this work are about 2 orders of magnitude higher than many of the ammonium and phosphonium salts in the $Cubb_{bi}$ phases.[11,12,16] Considering the inherent lability of the Ag−N bond, ionic conduction involving the migration of a Ag^I ion other than the bulky Ag_4-triazole cation cannot be ruled out. The dramatic enhancement of the ionic conductivity via doping of a small amount of $AgBF_4$ is presumable caused by the promotion of Ag^I ion migration in the 3D channel network. However, our data are still lower than that of the solid Ag^I (1.0 S/cm), in which silver ions are hopping through crystal defect.[85−87] Therefore, how to increase the density of mobile Ag^I ions in the channel to enhance the ionic conductivity remains to be studied.

3. CONCLUSIONS

LCs of tetranuclear Ag_4-triazole compounds are prepared. These compounds have a rodlike cation composed of an antiprismatic rigid ionic core in the center and six flexible alkyl chains, three each related by a center of inversion pointing above and below the core. All of these compounds undergo a phase transition upon heating in the sequence Cr → SmC → Cub → SmA → isotropic liquid. Depending on the chain length, two different types of cubic phases are observed. Those with shorter alkyl chains exhibit a micellar *Pm*3*n* cubic phase, whereas a bicontinuous *Ia*3*d* cubic phase is found for those with larger chains. The ionic conductivities in the Cub_{bi} phase, especially in the addition of a small amount of $AgBF_4$, are superior to those of ammonium and phosphonium salts. The three-dimensionally interconnected ion nanochannel networks together with the inherent lability of metal−ligand bonds may provide an efficient ion-transport property.

4. EXPERIMENTAL SECTION

Silver nitrate was purchased from RDH. Silver tetrafluoroborate was obtained from Alfa Aesar. The solvents were reagent-grade from Acros and Mallinckrodt Chemical Co. and were used without further purification. ^{1}H NMR spectra were recorded on Advanced DXP_{300} Bruker and DXP_{400} Bruker spectrometers with tetramethylsilane as an internal standard. Elemental microanalyses were performed by the Taiwan Instrumentation Center. Optical characterization of ligand crystals was performed on a ZEISS Axioplan2 imaging polarizing microscope equipped with a Mettler FP 82 hot stage and a Mettler FP 90 central processor. Phase-transition temperatures were determined by DSC using a Mettler TGA/SDTA 851 calorimeter calibrated with indium and tin standards in conjunction with a Mettler DSC 822 thermal analysis data station. PXRD analysis was performed at the National Synchrotron Radiation Research Center (NSRRC) and on D8 Advanced Bruker and XRD Rigaku D/max-2500 diffractometers using Cu Kα radiation. Single-crystal data collection was carried out on a Bruker SMART APEX II diffractometer equipped with a SMART CCD array detector with graphite-monochromatized Mo Kα radiation (λ = 0.71073 Å) in ϕ and ω scan modes. All of the structures were solved and refined by a full-matrix least-squares method (based on F^2 using all independent data) employing *SHELXS-97* and *SHELXL-97* programs.[88] The ionic conductivity measurement was carried out under air with an impedance analyzer (Electrochemical Analyzer model 600C series).

4-Alkyl-1,2,4-triazoles (L^4-C_n, with n = 12, 14, 16, and 18). L^4-C_n ligands could be obtained from hydrazine monohydrate, ethyl formate, triethyl orthoformate, and primary *n*-alkylamines by Bayer synthesis.[56,89]

$[Ag_4(L^4\text{-}C_{18})_6][BF_4]_4$. 4-Octadecanyl-1,2,4-triazole (0.2 g, 0.62 mmol) in CH_2Cl_2 (20 mL) at room temperature and $AgBF_4$ (0.08 g, 0.41 mmol) in MeOH (10 mL) were mixed in the dark. The mixture was stirred and allowed to react for about 10 min. The solvent was then removed by rotary evaporation. The white powder was recrystallized from dichloromethane−diethyl ether (yield: 0.2 g, 71%). ^{1}H NMR ($CDCl_3$): δ 0.87 (t, ^3J = 6.6 Hz, 18H, CH_3), 1.24−1.30 (m, 180H, CH_2), 1.81 (m, 12H, CH_2), 4.05 (t, ^3J = 7.5 Hz, 12H, CH_2), 8.68 (s, 12H, CH). Elem anal. Calcd for $C_{120}H_{234}Ag_4B_4F_{16}N_{18}$: C, 53.22; H, 8.71; N, 9.31. Found: C, 53.62; H, 8.41; N, 8.89.

$[Ag_4(L^4\text{-}C_{16})_6][BF_4]_4$. This was obtained as a white powder. Yield: 0.25 g, 87%. ^{1}H NMR ($CDCl_3$): δ 0.87 (t, ^3J = 6.5 Hz, 18H, CH_3), 1.25−1.30 (m, 156H, CH_2), 1.83 (m, 12H, CH_2), 4.10 (t, ^3J = 7.3 Hz, 12H, CH_2), 8.72 (s, 12H, CH). Elem anal. Calcd for

dx.doi.org/10.1021/ic500627d | *Inorg. Chem.* 2014, 53, 5902−5910

$C_{108}H_{210}Ag_4B_4F_{16}N_{18}$: C, 51.08; H, 8.33; N, 9.93. Found: C, 51.01; H, 7.99; N, 9.62.

$[Ag_4(L^4\text{-}C_{14})_6][BF_4]_4$. This was obtained as a white powder. Yield: 0.25 g, 84%. ^{1}H NMR ($CDCl_3$): 0.87 (t, ^3J = 6.4 Hz, 18H, CH_3), 1.24−1.30 (m, 132H, CH_2), 1.82 (m, 12H, CH_2), 4.09 (t, ^3J = 7.2 Hz, 12H, CH_2), 8.72 (s, 12H, CH). Elem anal. Calcd for $C_{96}H_{186}Ag_4B_4F_{16}N_{18}$: C, 48.62; H, 7.91; N, 10.63. Found: C, 48.60; H, 8.07; N, 10.45.

$[Ag_4(L^4\text{-}C_{12})_6][BF_4]_4$. This was obtained as a white powder. Yield: 0.22 g, 71%. ^{1}H NMR ($CDCl_3$): δ 0..87 (t, ^3J = 6.6 Hz, 18H, CH_3), 1.24−1.30 (m, 108H, CH_2), 1.82 (m, 12H, CH_2), 4.05 (t, ^3J = 7.6 Hz, 12H, CH_2), 8.72 (s, 12H, CH). Elem anal. Calcd for $C_{84}H_{162}Ag_4B_4F_{16}N_{18}$: C, 45.80; H, 7.41; N, 11.44. Found: C, 45.75; H, 7.13; N, 11.21.

■ ASSOCIATED CONTENT

Supporting Information

X-ray crystallographic file in CIFformat, crystal structure data, phase transition analysis, powder XRD data, and experimental section. This material is available free of charge via the Internet at http://pubs.acs.org.

■ AUTHOR INFORMATION

Corresponding Author

*E-mail: ijblin@mail.ndhu.edu.tw.

Notes

The authors declare no competing financial interest.

■ ACKNOWLEDGMENTS

We thank the National Science Council (NSC) of Taiwan for financial support (NSC 102-2113-M-259-002) and the National Synchrotron Radiation Research Center of Taiwan (NSRRC) for providing research facilities.

■ REFERENCES

(1) Tschierske, C. *Angew. Chem., Int. Ed.* **2013**, *52*, 8828.
(2) Kato, T.; Mizoshita, N.; Kishimoto, K. *Angew. Chem., Int. Ed.* **2006**, *45*, 38.
(3) Axenov, K. V.; Laschat, S. *Materials* **2011**, *4*, 206.
(4) Kutsumizu, S. *Isr. J. Chem.* **2012**, *52*, 844.
(5) Binnemans, K. *Chem. Rev.* **2005**, *105*, 4148.
(6) Gray, G. W.; Jones, B.; Marson, F. *J. Chem. Soc.* **1957**, 393.
(7) Diele, S. *Curr. Opin. Colloid Interface Sci.* **2002**, *7*, 333.
(8) Impéror-Clerc, M. *Curr. Opin. Colloid Interface Sci.* **2005**, *9*, 370.
(9) Kutsumizu, S. *Curr. Opin. Solid State Mater. Sci.* **2002**, *6*, 537.
(10) Gray, G. W. *Smectic Liquid Crystals, Textures and Structure*; Leonard Hill: Glasgow, U.K., 1984; p 68.
(11) Ichikawa, T.; Yoshio, M.; Hamasaki, A.; Mukai, T.; Ohno, H.; Kato, T. *J. Am. Chem. Soc.* **2007**, *129*, 10662.
(12) Ichikawa, T.; Yoshio, M.; Hamasaki, A.; Taguchi, S.; Liu, F.; Zeng, X.-b.; Ungar, G.; Ohno, H.; Kato, T. *J. Am. Chem. Soc.* **2012**, *134*, 2634.
(13) Frise, A. E.; Ichikawa, T.; Yoshio, M.; Ohno, H.; Dvinskikh, S. V.; Kato, T.; Furo, I. *Chem. Commun.* **2010**, *46*, 728.
(14) Soberats, B.; Yoshio, M.; Ichikawa, T.; Taguchi, S.; Ohno, H.; Kato, T. *J. Am. Chem. Soc.* **2013**, *135*, 15286.
(15) Cho, B.-K.; Jain, A.; Gruner, S. M.; Wiesner, U. *Science* **2004**, *305*, 1598.
(16) Ichikawa, T.; Yoshio, M.; Hamasaki, A.; Kagimoto, J.; Ohno, H.; Kato, T. *J. Am. Chem. Soc.* **2011**, *133*, 2163.
(17) Kishimoto, K.; Suzawa, T.; Yokota, T.; Mukai, T.; Ohno, H.; Kato, T. *J. Am. Chem. Soc.* **2005**, *127*, 15618.
(18) Yoshio, M.; Ichikawa, T.; Shimura, H.; Kagata, T.; Hamasaki, A.; Mukai, T.; Ohno, H.; Kato, T. *Bull. Chem. Soc. Jpn.* **2007**, *80*, 1836.
(19) Percec, V.; Johansson, G.; Heck, J.; Ungarb, G.; Battyb, S. V. *J. Chem. Soc., Perkin Trans. 1* **1993**, 1411.
(20) Binnemans, K. *J. Mater. Chem.* **2009**, *19*, 448.
(21) Barberá, J.; Lantero, I.; Moyano, S.; Serrano, J. L.; Elduque, A.; Giménez, R. *Chem.—Eur. J.* **2010**, *16*, 14545.
(22) Mayoral, M. J.; Ovejero, P.; Campo, J. A.; Heras, J. V.; Torres, M. R.; Lodeiro, C.; Cano, M. *New J. Chem.* **2010**, *34*, 2766.
(23) Ovejero, P.; Asensio, E.; Heras, J. V.; Campo, J. A.; Cano, M.; Torres, M. R.; Nunez, C.; Lodeiro, C. *Dalton Trans.* **2013**, *42*, 2107.
(24) Serrano, J. L. *Metallomesogens: Synthesis, Properties, and Applications*; Wiley-VCH: Weinheim, Germany, 1996.
(25) Bruce, D. W. *Acc. Chem. Res.* **2000**, *33*, 831.
(26) Serrano, J. L. *Metallomesogens: Synthesis, Properties, and Applications*; Wiley-VCH Verlag GmbH: Berlin, 2007.
(27) Pucci, D.; Barberio, G.; Bellusci, A.; Crispini, A.; Donnio, B.; Giorgini, L.; Ghedini, M.; La Deda, M.; Szerb, E. I. *Chem.—Eur. J.* **2006**, *12*, 6738.
(28) Mayoral, M. J.; Ovejero, P.; Campo, J. A.; Heras, J. V.; Pinilla, E.; Torres, M. R.; Lodeiro, C.; Cano, M. *Dalton Trans.* **2008**, 6912.
(29) Lee, C. K.; Hsu, K.-M.; Tsai, C.-H.; Lai, C. K.; Lin, I. J. B. *Dalton Trans.* **2004**, 1120.
(30) Hsu, T. H. T.; Naidu, J. J.; Yang, B.-J.; Jang, M.-Y.; Lin, I. J. B. *Inorg. Chem.* **2012**, *51*, 98.
(31) Cardinaels, T.; Ramaekers, J.; Nockemann, P.; Driesen, K.; Van Hecke, K.; Van Meervelt, L.; Lei, S.; De Feyter, S.; Guillon, D.; Donnio, B.; Binnemans, K. *Chem. Mater.* **2008**, *20*, 1278.
(32) Binnemans, K.; Görller-Walrand, C. *Chem. Rev.* **2002**, *102*, 2303.
(33) Demus, D.; Goodby, J. W.; Gray, G. W.; Spiess, H. W.; Vill, V. *Handbook of Liquid Crystals*; Wiley-VCH: Weinheim, Germany, 1998; Vols. *1*−*3*.
(34) Espinet, P.; Esteruelas, M. A.; Oro, L. A.; Serrano, J. L.; Sola, E. *Coord. Chem. Rev.* **1992**, *117*, 215.
(35) Chico, R. n.; Castillejos, E.; Serp, P.; Coco, S.; Espinet, P. *Inorg. Chem.* **2011**, *50*, 8654.
(36) Cavero, E.; Uriel, S.; Romero, P.; Serrano, J. L.; Giménez, R. *J. Am. Chem. Soc.* **2007**, *129*, 11608.
(37) Matsukizono, H.; Kuroiwa, K.; Kimizuka, N. *J. Am. Chem. Soc.* **2008**, *130*, 5622.
(38) Kuroiwa, K.; Shibata, T.; Takada, A.; Nemoto, N.; Kimizuka, N. *J. Am. Chem. Soc.* **2004**, *126*, 2016.
(39) Kuroiwa, K.; Shibata, T.; Sasaki, S.; Ohba, M.; Takahara, A.; Kunitake, T.; Kimizuka, N. *J. Polym. Sci., Polym. Chem.* **2006**, *44*, 5192.
(40) Carmen Lequerica, M. d.; Baena, M. J.; Espinet, P. *Inorg. Chim. Acta* **2008**, *361*, 2270.
(41) Hui, J. K. H.; MacLachlan, M. J. *Coord. Chem. Rev.* **2010**, *254*, 2363.
(42) Matsukizono, H.; Kuroiwa, K.; Kimizuka, N. *Chem. Lett.* **2008**, *37*, 446.
(43) Kuroiwa, K.; Kimizuka, N. *Chem. Lett.* **2008**, *37*, 192.
(44) Kume, S.; Kuroiwa, K.; Kimizuka, N. *Chem. Commun.* **2006**, 2442.
(45) Coco, S.; Cordovilla, C.; Donnio, B.; Espinet, P.; García-Casas, M. J.; Guillon, D. *Chem.—Eur. J.* **2008**, *14*, 3544.
(46) Seo, J.-S.; Yoo, Y.-S.; Choi, M.-G. *J. Mater. Chem.* **2001**, *11*, 1332.
(47) Mukai, H.; Yokokawa, M.; Ichihara, M.; Hatsusaka, K.; Ohta, K. *J. Porphyrins Phthalocyanines* **2010**, *14*, 188.
(48) Ichihara, M.; Suzuki, A.; Hatsusaka, K.; Ohta, K. *Liq. Cryst.* **2007**, *34*, 555.
(49) Terazzi, E.; Bourgogne, C.; Welter, R.; Gallani, J.-L.; Guillon, D.; Rogez, G.; Donnio, B. *Angew. Chem., Int. Ed.* **2008**, *47*, 490.
(50) Goossens, K.; Bruce, D. W.; Van Deun, R.; Binnemans, K.; Cardinaels, T. *Dalton Trans.* **2012**, *41*, 13271.
(51) Mukai, H.; Yokokawa, M.; Ichihara, M.; Hatsusaka, K.; Ohta, K. *J. Porphyrins Phthalocyanines* **2010**, *14*, 188.
(52) Grondin, P.; Siretanu, D.; Roubeau, O.; Achard, M.-F.; Clérac, R. *Inorg. Chem.* **2012**, *51*, 5417.
(53) Seredyuk, M.; Gaspar, A. B.; Ksenofontov, V.; Galyametdinov, Y.; Verdaguer, M.; Villain, F.; Gütlich, P. *Inorg. Chem.* **2008**, *47*, 10232.

(54) Seredyuk, M.; Gaspar, A. B.; Ksenofontov, V.; Reiman, S.; Galyametdinov, Y.; Haase, W.; Rentschler, E.; Gütlich, P. *Chem. Mater.* **2006**, *18*, 2513.
(55) Roubeau, O. *Chem.—Eur. J.* **2012**, *18*, 15230.
(56) Roubeau, O.; Alcazar Gomez, J. M.; Balskus, E.; Kolnaar, J. J. A.; Haasnoot, J. G.; Reedijk, J. *New J. Chem.* **2001**, *25*, 144.
(57) Shao, S. C.; Zhu, D. R.; Zhu, X. H.; You, X. Z.; Shanmuga Sundara Raj, S.; Fun, H. K. *Acta Crystallogr., Sect. C* **1999**, *55*, 1412.
(58) Sun, Q.; Zheng, F.; Sun, X.; Wang, W. *Acta Crystallogr., Sect. E: Struct. Rep. Online* **2009**, *65*, m283.
(59) Wang, Y.; Ding, B.; Cheng, P.; Liao, D.-Z.; Yan, S.-P. *Inorg. Chem.* **2007**, *46*, 2002.
(60) Wang, Y.; Cheng, P. *Struct. Chem.* **2007**, *18*, 677.
(61) Shao, S.-C.; You, Z.-L.; Zhang, S.-P.; Zhu, H.-L.; Ng, S. W. *Acta Crystallogr.. Sect. E: Struct. Rep. Online* **2005**, *61*, m265.
(62) Jia-Cheng, L.; Guo-Cong, G.; Hong-Wei, M.; Chun, Y.; Guo-Wei, Z.; Fa-Kun, Z.; Shan-Huo, L.; Ming-Sheng, W.; Jin-Shun, H. *Chin. J. Struct. Chem.* **2002**, *21*, 371.
(63) Yang, G.; Wang, Y.-L.; Liu, L.-L.; Ng, S. *Transition Met. Chem.* **2009**, *34*, 751.
(64) Wang, Y.-L.; Yang, G.; Ng, S. W. *Acta Crystallogr., Sect. E: Struct. Rep. Online* **2007**, *63*, m1801.
(65) Wang, Y.; Yi, L.; Yang, X.; Ding, B.; Cheng, P.; Liao, D.-Z.; Yan, S.-P. *Inorg. Chem.* **2006**, *45*, 5822.
(66) Liu, B.; Xu, L.; Guo, G.-C.; Huang, J.-S. *Inorg. Chem. Commun.* **2006**, *9*, 687.
(67) Massiot, P.; Impéror-Clerc, M.; Veber, M.; Deschenaux, R. *Chem. Mater.* **2005**, *17*, 1946.
(68) Seddon, J. M.; Robins, J.; Gulik-Krzywicki, T.; Delacroix, H. *Phys. Chem. Chem. Phys.* **2000**, *2*, 4485.
(69) Hudson, S. D.; Jung, H.-T.; Percec, V.; Cho, W.-D.; Johansson, G.; Ungar, G.; Balagurusamy, V. S. K. *Science* **1997**, *278*, 449.
(70) Li, X.; Kunieda, H. *Langmuir* **2000**, *16*, 10092.
(71) Jiménez, J.; Laguna, A.; Molter, A. M.; Serrano, J. L.; Barberá, J.; Oriol, L. *Chem.—Eur. J.* **2011**, *17*, 1029.
(72) Dukeson, D. R.; Ungar, G.; Balagurusamy, V. S. K.; Percec, V.; Johansson, G. A.; Glodde, M. *J. Am. Chem. Soc.* **2003**, *125*, 15974.
(73) Tseng, J. C. W.; Rondla, R.; Su, P. Y. S.; Lin, I. J. B. *RSC Adv.* **2013**, *3*, 25151.
(74) Bruce, D. W.; Dunmur, D. A.; Hudson, S. A.; Lalinde, E.; Maitlis, P. M.; Malcolm, P.; McDonald, M. P.; Orr, R.; Styring, P.; Cherodian, A. S.; Richardson, R. M.; Feijoo, J. L.; Ungar, G. *Mol. Cryst. Liq. Cryst.* **1991**, *206*, 79.
(75) Borisch, K.; Diele, S.; Goring, P.; Kresse, H.; Tschierske, C. *J. Mater. Chem.* **1998**, *8*, 529.
(76) Seo, S. H.; Park, J. H.; Tew, G. N.; Chang, J. Y. *Tetrahedron Lett.* **2007**, *48*, 6839.
(77) Percec, V.; Cho, W.-D.; Ungar, G.; Yeardley, D. J. P. *J. Am. Chem. Soc.* **2001**, *123*, 1302.
(78) Cheng, X.; Bai, X.; Jing, S.; Ebert, H.; Prehm, M.; Tschierske, C. *Chem.—Eur. J.* **2010**, *16*, 4588.
(79) Cheng, X.; Su, F.; Huang, R.; Gao, H.; Prehm, M.; Tschierske, C. *Soft Matter* **2012**, *8*, 2274.
(80) Dai, H.; Yang, X.; Tan, X.; Su, F.; Cheng, X.; Liu, F.; Tschierske, C. *Chem. Commun.* **2013**, *49*, 10617.
(81) Tan, X.; Kong, L.; Dai, H.; Cheng, X.; Liu, F.; Tschierske, C. *Chem.—Eur. J.* **2013**, *19*, 16303.
(82) Macdonald, J. R. *Impedance Spectroscopy: Emphasizing Solid Materials and Systems*; John Wiley & Sons: New York, 1987.
(83) Yoshio, M.; Mukai, T.; Kanie, K.; Yoshizawa, M.; Ohno, H.; Kato, T. *Adv. Mater.* **2002**, *14*, 351.
(84) Adams, H.; Bailey, N. A.; Bruce, D. W.; Davis, S. C.; Dunmur, D. A.; Hempstead, P. D.; Hudson, S. A.; Thorpe, S. *J. Mater. Chem.* **1992**, *2*, 395.
(85) Govindacharyulu, P. A.; Bose, D. N.; Suri, S. K. *J. Phys. Chem. Solids* **1978**, *39*, 961.
(86) Turbandt, C.; Lorentz, E. *Z. Phys. Chem.* **1914**, *87*, 513.
(87) Turbandt, C.; Lorentz, E. *Z. Phys. Chem.* **1914**, *87*, 543.
(88) Sheldrick, G. *Acta Crystallogr., Sect. A* **2008**, *64*, 112.
(89) Bayer, H. O.; Cook, R. S.; von Mayer, W. C. U.S. Patent 3,798,276, 1974.